

Non-reciprocal Magnetoresistances in Chiral Tellurium

Shuchen Li,¹ Chang Niu,^{2,3} Peide D. Ye,^{2,3} and Axel Hoffmann^{4, a)}

¹⁾Department of Materials Science and Engineering and Materials Research Laboratory, The Grainger College of Engineering, University of Illinois Urbana-Champaign, Urbana, Illinois 61801, USA

²⁾Birck Nanotechnology Center, Purdue University, West Lafayette, IN 47907, United States.

³⁾Elmore Family School of Electrical and Computer Engineering, Purdue University, West Lafayette, IN 47907, United States.

⁴⁾Department of Materials Science and Engineering and Materials Research Laboratory, University of Illinois Urbana-Champaign, Urbana, Illinois 61801, USA

Materials with broken fundamental symmetries, such as chiral crystals, provide a rich playground for exploring unconventional spin-dependent transport phenomena. The interplay between a material's chirality, strong spin-orbit coupling, and charge currents can lead to complex non-reciprocal effects, where electrical resistance depends on the direction of current and magnetic fields. In this study, we systematically investigate the angular dependencies of magnetoresistance in single-crystalline chiral Tellurium (Te). We observe distinct non-reciprocal magnetoresistances for magnetic fields applied along three orthogonal directions: parallel to the current along the chiral axis (**z**), in the sample plane but perpendicular to the current (**y**), and out of the sample plane (**x**). Through detailed analysis of the chirality- and thickness-dependence of the signals, we successfully disentangle multiple coexisting mechanisms. We conclude that the Edelstein effect, arising from the chiral structure's radial spin texture, is responsible for the non-reciprocity along the **z**-axis. In contrast, the chirality-independent signal along the **y**-axis is attributed to the Nernst effect, and the non-reciprocity along the **x**-axis may originate from intrinsic orbital magnetizations. These findings elucidate the complex interplay of spin, orbital, and thermal effects in Te, providing a complete picture of its non-reciprocal transport properties.

I. INTRODUCTION

The breaking of fundamental symmetries in crystalline solids is a cornerstone for the discovery and manipulation of novel quantum phenomena¹. In materials that lack a center of inversion, the interplay between the spin of an electron and its momentum, governed by strong spin-orbit coupling (SOC), gives rise to a host of unconventional transport effects that are forbidden in centrosymmetric systems^{2–5}. One of the most fascinating of these is non-reciprocal charge transport, where the electrical resistance is not the same when the current direction is reversed. This effect serves as a powerful probe of symmetry-breaking and has significant potential for applications in next-generation electronics^{6,7}.

A primary mechanism for generating non-reciprocal transport is through the creation of a net spin polarization in the material. In systems with strong Rashba-type SOC, such as the polar semiconductor BiTeBr, an applied magnetic field can asymmetrically shift the spin-split Fermi surfaces, leading to a current-direction-dependent resistance, often termed unidirectional magnetoresistance (UMR) or bilinear magnetoelectric resistance⁸. This effect can be intuitively understood as the interplay between the external magnetic field and current-induced net spin polarizations that arise from the out-of-equilibrium shift of the spin-momentum-locked Fermi

contours^{6,9}. The magnitude of this non-reciprocity is directly tied to the strength of the underlying spin-orbit interaction, making it a valuable tool for quantifying spin-splitting. Moreover, its detailed angular dependence makes UMR an exceptionally sensitive probe of the complete three-dimensional spin texture, capable of revealing complex features beyond the standard Rashba model, such as the momentum-dependent out-of-plane spin components observed in SrTiO₃ based 2 dimensional electron gas¹⁰.

Another key mechanism for non-reciprocal transport arises from the intrinsic handedness of a material's crystal structure. In chiral systems, which lack all mirror symmetries, the combination of structural chirality and a magnetic field can lead to a phenomenon known as magnetochiral anisotropy^{11,12}. This effect manifests as a correction to the resistance that is linear in both the applied current and the magnetic field, and its sign depends on the handedness of the crystal¹³. This behavior is distinct from polarization-induced effects and provides an alternative route to achieving current-direction-dependent transport, driven by the interplay between the chiral structures, magnetic field, and electron's spin.

Tellurium (Te), an elemental material that has a chiral crystal structure with three tellurium atoms forming a spiral-shaped covalently bonded atomic chain in each unit cell, stands out as a compelling material for exploring non-reciprocal transport through the interplay among structural chirality and strong SOC^{14–16}. The helicity of this atomic chain imparts a well-defined chirality, breaking both inversion and mirror symmetries. This unique

^{a)}Electronic mail: axelh@illinois.edu

crystallographic property, combined with a strong intrinsic SOC, lifts spin degeneracy and leads to a complex band structure with a radial spin texture at the Fermi surface. When a charge current is applied along the chiral axis, the Edelstein effect is predicted to induce a net spin polarization collinear with the current, with opposite polarities for right- and left-handed Te¹⁷ as shown in Fig. 1 (a), also making Te an ideal platform for investigating novel spintronic phenomena. This is a critical goal for developing next-generation, low-power electronic devices^{18–20}. Moreover, with an application of an external magnetic field, non-reciprocal magnetoresistance have been found and reported in Te, while a comprehensive understanding of how structural chirality governs magnetotransport responses under various magnetic field orientations is still developing^{14,18,20–22}. In this paper, we systematically investigate the non-reciprocal magnetoresistance in single-crystalline Te. We identify and disentangle three distinct non-reciprocal effects by analyzing their unique dependencies on crystal chirality, sample thickness, and magnetic field direction, attributing their origins to the Edelstein effect, the Nernst effect^{3,23}, and intrinsic orbital magnetization^{24,25}, respectively.

II. MEASUREMENT

Single crystalline Te flakes were grown by using the hydrothermal method²⁰, and we used lithography and deposited Pt electrodes for transport measurements, in which a current is applied along $+z$, and $y(x)$ direction is orthogonal to the current-direction in (out) of the device plane[Fig. 1 (b)]. At the same time, a magnetic field B is applied in the $zy(xz, xy)$ plane, and we detected the longitudinal resistance using a lock-in amplifier at various angles $\phi(\beta, \gamma)$, where $\phi(\beta, \gamma)$ is the angle between B and $+z(+x,+x)$. In this paper, $\phi(\beta, \gamma) = 0^\circ$ when B is parallel to $+z(+x,+x)$ and $\phi(\beta, \gamma) = 90^\circ$ when B along $+y(+z,+y)$ axis, as shown in Fig. 1 (c).

We started our measurement by applying an ac current $I_0 \sin(\omega t)$ along the chiral axis of Te (R1) and collected the longitudinal first harmonic signal V_0^ω as we rotated the magnetic field both in the ϕ and β plane. As shown in Fig. 2 (a) and (d), we plot $\Delta V_0^\omega = V_0^\omega - V_{0,average}^\omega$ as a function of ϕ and β , and we found Te has largest magnetoresistance when B is out-of-plane along x and smallest when B is parallel with the chiral axis and the

current direction.

We then applied a positive dc offset I_{dc} to the ac current, with $I = I_0 \sin(\omega t) + I_{dc}$, and $I_0 = |I_{dc}|$, and performed similar ϕ and β scans. Interestingly, as shown in Fig. 2 (b) and (e), we found the angular dependencies(orange curves) of $\Delta V_{I+}^\omega = V_{I+}^\omega - V_{I+,average}^\omega$ were drastically changed with the application of a positive dc offset, and Te magnetoresistances were no longer even with the field, with clear non-reciprocal features appearing in both ϕ and β scans. Specifically, in ϕ scan, we found V_{I+}^ω is smaller when the B is parallel to the current

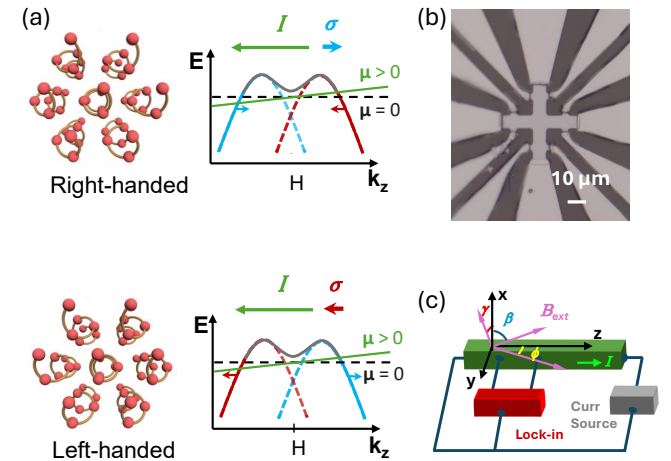


FIG. 1. (a)Diagrams showing left-handed and right-handed Te crystal structures and the corresponding spin polarizations due to Edelstein effect.(b)Microscopic image of a fabricated Te device, with current channels both along and perpendicular to the chiral axis. (c)Schematics showing the measurement setup under various field scans.

direction ($\phi = 0^\circ$) and larger when they are antiparallel ($\phi = 180^\circ$). Surprisingly, we have also observed a difference in ΔV_{I+}^ω when $\phi = 90^\circ$ and 270° , with a smaller ΔV_{I+}^ω at $\phi = 90^\circ$. The two non-reciprocal behaviors of magnetoresistance in ϕ scan also appear in β scans at $\beta = 90^\circ$ and 270° . Remarkably, we also observed another non-reciprocal behavior when the field is along x out-of-plane, as ΔV_{I+}^ω at $\beta = 0^\circ$ and 180° is different. We then reversed the current direction by applying a negative I_{dc} and observed behaviors of ΔV_{I-}^ω also reversed(purple curves in Fig. 2 (d) and (e)) as expected.

Based on our experimental observations, we generalized the electrical resistance of Te as

$$R(I, B) = R_0[1 + B^2(\delta_z \cos \phi \sin(\theta) + \delta_y \sin \theta \sin \phi + \delta_x \cos \theta)^2 + \rho I^2] + IB(\alpha_z \sin \theta \cos \phi + \alpha_y \sin \theta \sin \phi + \alpha_x \cos \phi) \quad (1)$$

where R_0 , I , and B represent the resistance of Te at zero field, the current, and the external magnetic field. The coefficients δ_z , δ_y , and δ_x correspond to the normal magnetoresistances of Te when B is along z , y , and x that

will cause R to either decrease or increase with the field, and are independent of current. On the other hand, α_z , α_y , and α_x correspond to the sizes of the non-reciprocal effects in Te for B along z , y , and x , which are dependent

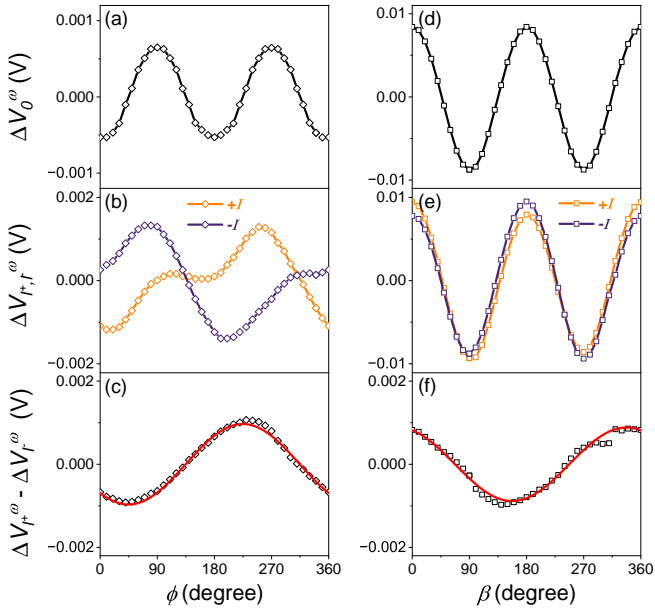


FIG. 2. (a) and (d) β and ϕ scans of mangetoresistance of Te with pure ac currents. (b) and (e) ϕ , β scans of Te with positive (orange) and negative (purple) dc offsets. (c) and (f) Angular dependencies of $\Delta V_{I+}^\omega - \Delta V_{I-}^\omega$ to extract components with sine and cosine angular dependencies.

on both B and I , rectifying Te magnetoresistances. ρ is the coefficient for thermal effect.

Thus, when we applied a dc offset with $I = I_0 \sin(\omega t) + I_{dc}$, the resultant longitudinal first harmonic signal V^ω would also be modified (see supplemental materials), giving rise to the observed non-reciprocal effects. To exclude other contributions in Te, we calculated and plotted $\Delta V_{I+}^\omega - \Delta V_{I-}^\omega$ under the same field but opposite dc offsets in Fig. 2 (c) and (f), and extracted $\alpha_z = -3.1 \pm 0.2 \text{ k}\Omega/(A \cdot T)$, $\alpha_y = -3.6 \pm 0.2 \text{ k}\Omega/(A \cdot T)$, and $\alpha_x = 3.8 \pm 0.2 \text{ k}\Omega/(A \cdot T)$ by using Eq. 1 from cosine and sine components in the ϕ and β dependencies of ΔV^ω easily.

It is instructive to study also the non-linear second harmonic signal $V^{2\omega}$ proportional to the current, which also reflects the non-reciprocal effects and is independent of I_{dc} , and the analysis of it can be complementary to that of V^ω . Fig. 3 (a)-(c) showed $\Delta V_B^{2\omega}$ of Te (R1) as a function of B_z , B_y , and B_x up to 9 T and 2 T due to system geometry restrictions, with various ac amplitude I_0 , where $\Delta V_B^{2\omega} = (V^{2\omega}(\pm B) - V^{2\omega}(\mp B))/2$ is the absolute change in second harmonic signal. Clear linear relationships with all B_z , B_y , and B_x can be observed from all I_0 , agreed well with Eq. 1, confirming three non-reciprocal behaviors observed in first harmonic magnetoresistance measurements. Fig. 3 (d) shows $\Delta V_B^{2\omega}/(I_0 B)$ as a function of I_0 for B_z (red), B_y (blue), and B_x (green), and the slopes are directly proportional to the sizes of α_z , α_y , and α_x . We calculated $\alpha_z = -3.2 \pm 0.1 \text{ k}\Omega/(A \cdot T)$, $\alpha_y = -7 \pm 0.1 \text{ k}\Omega/(A \cdot T)$, and $\alpha_x = 4.9 \pm 0.1 \text{ k}\Omega/(A \cdot T)$, comparable to the results derived from the magnetoresistance measurements. Similarly, we measured $V^{2\omega}$ for Te

(L1) as a function of I_0 and fields. Fig. 3 (e)-(g) showed $\Delta V_B^{2\omega}$ as a function of B_z , B_y , and B_x for different current densities along the chiral axis. Clearly, the slope of the B_z -dependency of $\Delta V_B^{2\omega}$ changed sign when Te chirality changed. However, the slope of B_y and B_x dependencies stayed the same. We then plot $\Delta V_B^{2\omega}/(I_0 B)$ as a function of I_0 in Fig. 3 (h) and extract α_z , α_y , and α_x to be $292.3 \pm 26.4 \text{ k}\Omega/(A \cdot T)$, $-187.1 \pm 19.2 \text{ k}\Omega/(A \cdot T)$, and $139.3 \pm 8.8 \text{ k}\Omega/(A \cdot T)$. We noticed a significant difference in the magnitudes of all coefficients between the two samples, which is likely related to their different resistances (1200Ω vs 17200Ω), so we studied the thickness dependence of α_z , α_y , and α_x by performing the second harmonic measurements across a wide range of Te samples with various thicknesses. Table I recorded the calculated coefficients together with the resistances of corresponding devices, which is directly related to the sample thicknesses. First, we found α_z indicates a clear chirality-dependent origin with both positive and negative signs among the samples, while α_y is always negative in all the samples measured, suggesting a chirality-independent origin. We also noticed that the sign of α_x also varied across different Te samples, but did not tie to that of α_z , which means α_x could have opposite signs even if α_z had the same sign, for example from device 1 and 2. We then plotted the ratio between absolute values of extracted α_z , α_y , and α_x and the corresponding device resistance R_0 as a function of R_0 in Fig. 4, the linear relationships for all three coefficients indicate intrinsic bulk origins behind.

Device	R_0 [$\text{k}\Omega$]	α_z [$\text{k}\Omega/(A \cdot T)$]	α_y [$\text{k}\Omega/(A \cdot T)$]	α_x [$\text{k}\Omega/(A \cdot T)$]
L1	17.2	292.3 ± 26.4	-187.1 ± 19.2	139.3 ± 8.8
L2	14.9	172 ± 8.1	-126.5 ± 13.5	-119.2 ± 15.5
R1	1.2	-3.2 ± 0.1	-7 ± 0.1	4.9 ± 0.1
R2	1.3	-6.6 ± 0.9	-9.2 ± 0.2	-8.5 ± 0.6
L3	1.8	50.8 ± 8.3	-23.3 ± 3.0	
L4	1.7	44.1 ± 1.1	-38.1 ± 3.0	-6.3 ± 1.1
R3	2.0	-13.2 ± 2.7	-32 ± 4.2	
L5	1.6	6.7 ± 1.0	-19.7 ± 1.3	
R4	2.6	-14.9 ± 2.2	-45.7 ± 6.1	-51.1 ± 4.4
R5	16.2	-196 ± 12.9	-122 ± 8.8	207.5 ± 14.5

TABLE I. Resistances R_0 of different Te devices and extracted non-reciprocal effect coefficients α_z , α_y , α_x from second harmonic voltages. Right or left chirality is indicated by R and L with the device number followed

III. DISCUSSION

We would like to discuss possible origins behind the non-reciprocal magnetoresistances observed in Te, for fields along **z**, **y** and **x** when current is along the chiral axis.

First, the non-reciprocal magnetoresistance along the

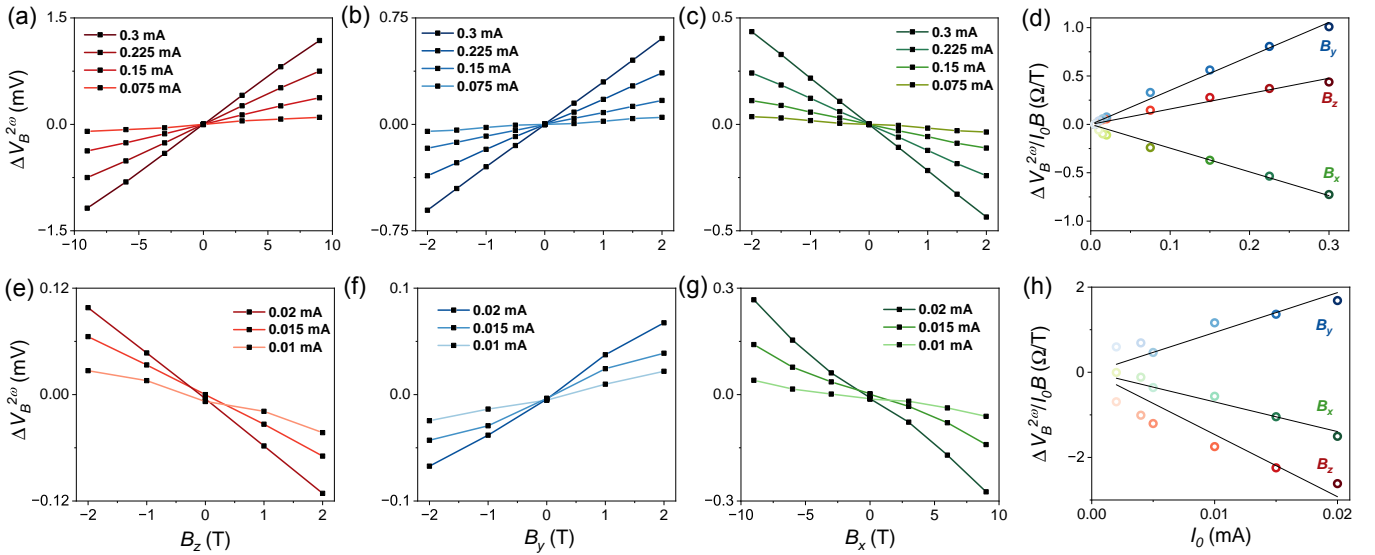


FIG. 3. (a)-(c) $\Delta V_B^{2\omega}$ under B_z , B_y , and B_x field sweep for Te(R1). (e)-(g) $\Delta V_B^{2\omega}$ under B_z , B_y , and B_x field sweep for Te(L1). (d) and (h) $\Delta V_B^{2\omega}/(I_0 B)$ vs current for Te(R1) and (L1). Red, blue, and green dots correspond to $\Delta V_B^{2\omega}/(I_0 B)$ at fields along B_z , B_y , and B_x at different current densities.

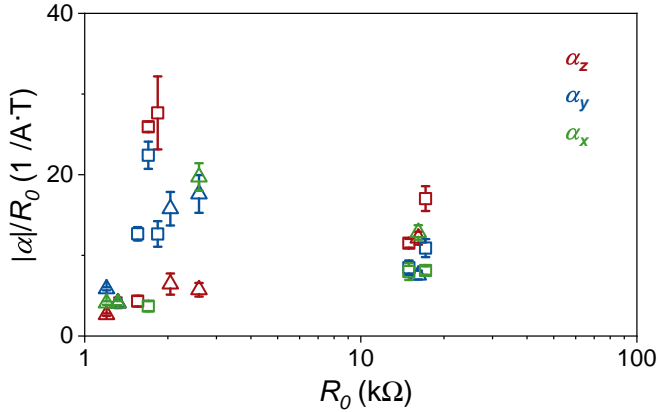


FIG. 4. Ratio of absolute values of extracted α_z , α_y , and α_x and the corresponding device resistance R_0 as a function of R_0 . Squares and triangles represent left and right handedness.

chiral axis displayed a clear chirality-dependent behavior which changed signs as we changed Te handedness, and we attributed that to the chirality-induced spin polarizations along the current directions due to the Edelstein effect and Te radial spin textures¹⁸. Also, magnitude of α_z decreased as Te thicknesses increased, further confirming the bulk effect from the radial spin textures.

However, the non-reciprocal magnetoresistances when B is along y that always had the same polarities regardless of the handedness, and the corresponding coefficient α_y is always negative for all the samples measured, strongly suggesting a chirality-independent origin behind, and we proposed Nernst effect could explain the observations, that is a thermal gradient ΔT generated out-of-plane could give rise to different magnetoresistances for $\pm B_y$, whose magnitude is proportional to

$\Delta T \times B_y$. We note that thermally generated ΔT does not reverse when we reversed the DC bias, and α_y would always be negative.

Finally, we attributed the non-reciprocal magnetoresistance when B is along x to the recently discovered orbital magnetization intrinsic to Te, that is along y , perpendicular to the chiral axis. Due to the distorted helix crystal structure of Te, two orbital magnetizations, M_y and M_z , arise from a simple helical tight-binding model²⁴. Thus, under an out-of-plane field B_x , a voltage $V_{orb,y} \propto M_y \times B_x$ will appear, giving rise to the observed non-reciprocity. Similar non-reciprocal behaviors should also occur when we applied B_x and a current perpendicular to the chiral axis, due to another orbital magnetization M_z , and as shown in Fig. 5 (c), we did observe a second harmonic voltage increased with both B_x and I_0 , confirming the two orbital magnetizations M_y and M_z in Te. Moreover, we also observed a similar second harmonic voltage under B_y field sweep when the current direction is perpendicular to the chiral axis due to the Nernst effect [Fig. 5 (b)]. However, we found no or negligibly small $V^{2\omega}$ under B_z perpendicular to the chiral axis, indicating a non-uniform radial spin texture in Te with much smaller current-induced spin polarizations perpendicular to the chiral axis [Fig. 5 (a)]. The magnitude of α_x is extracted to be 231.7 ± 14.7 $k\Omega/(A \cdot T)$ from fitting the slope of $\Delta V_B^{2\omega}/(I_0 B)$ in Fig. 5 (d).

IV. CONCLUSION

In summary, we have systematically characterized the angular-dependent magnetoresistance in single-crystalline chiral Te flakes. Our measurements reveal three distinct non-reciprocal transport phenomena when

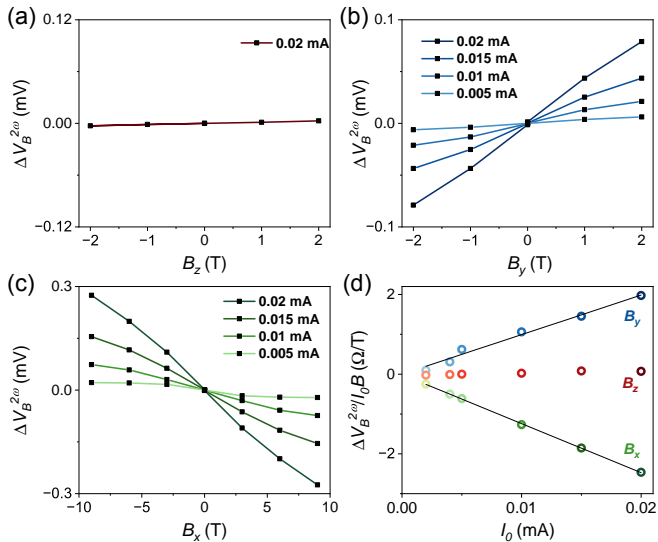


FIG. 5. (a), (b), and (c) $\Delta V_B^{2\omega}$ as a function of B_z , B_x , and B_y for current along \mathbf{z} for Te (L1), perpendicular to the chiral axis. (d) $\Delta V_B^{2\omega}/(I_0 B)$ vs current. Red, blue, and green dots correspond to $\Delta V_B^{2\omega}/(I_0 B)$ at fields along B_z , B_y , and B_x at different current densities.

a current is applied along the chiral axis. We have successfully disentangled their physical origins based on their unique dependencies on crystal chirality and magnetic field orientation. The chirality-dependent non-reciprocity along the transport direction is attributed to the Edelstein effect acting on the radial spin texture of Te's surface states. A second, chirality-independent effect is explained by the Nernst effect arising from a thermally generated gradient. Finally, a third non-reciprocity, observed with an out-of-plane field, is consistent with the influence of an intrinsic orbital magnetization. The pronounced thickness dependence of both the Edelstein effect and the orbital magnetization contributions underscores their origin at the bulk of the material. These findings not only provide a comprehensive picture of the complex interplay between charge, spin, and orbital degrees of freedom in a chiral conductor but also highlight the potential of tellurium for developing novel spintronic and orbitronic devices.

V. ACKNOWLEDGEMENTS

The authors would like to thank Paul Rutherford, Mandela Mehraeen, and Shulei Zhang (Case Western Reserve University) for insightful discussions regarding the origins behind Te's non-reciprocal magnetoresistance behaviors, and Ruihao Liu (Tsinghua University) for initiating the discussion between the authors and fostering this collaborative work. Support for the magnetoresistance measurements, data analysis, and manuscript preparation was provided by the Air Force Office of Scientific Research (AFOSR) MURI program under award

number FA9550-23-1-0311.

- ¹I. Žutić, J. Fabian, and S. Das Sarma, "Spintronics: Fundamentals and applications," *Rev. Mod. Phys.* **76**, 323–410 (2004).
- ²A. Manchon, H. C. Koo, J. Nitta, S. M. Frolov, and R. A. Duine, "New perspectives for rashba spin–orbit coupling," *Nature Materials* **14**, 871–882 (2015).
- ³T. Kikkawa, K. Uchida, Y. Shiomi, Z. Qiu, D. Hou, D. Tian, H. Nakayama, X.-F. Jin, and E. Saitoh, "Longitudinal spin seebeck effect free from the proximity nernst effect," *Phys. Rev. Lett.* **110**, 067207 (2013).
- ⁴R. Klause, S. Li, Y. Xiao, J. Gibbons, H.-C. Ni, J. Qian, J.-M. Zuo, E. E. Fullerton, and A. Hoffmann, "Unconventional spin-orbit torques due to reduced crystal symmetries," *IEEE Transactions on Magnetics* **61**, 1–7 (2025).
- ⁵R. Klause, Y. Xiao, J. Gibbons, V. P. Amin, K. D. Belashchenko, D. Go, E. E. Fullerton, and A. Hoffmann, "Unconventional field-like spin torques in crpt₃," *Phys. Rev. Appl.* **22**, 044043 (2024).
- ⁶P. He, S. S.-L. Zhang, D. Zhu, Y. Liu, Y. Wang, J. Yu, G. Vignale, and H. Yang, "Bilinear magnetoelectric resistance as a probe of three-dimensional spin texture in topological surface states," *Nature Physics* **14**, 495–499 (2018).
- ⁷Y. Tokura and N. Nagaosa, "Nonreciprocal responses from non-centrosymmetric quantum materials," *Nature Communications* **9**, 3740 (2018).
- ⁸T. Ideue, K. Hamamoto, S. Koshikawa, M. Ezawa, S. Shimizu, Y. Kaneko, Y. Tokura, N. Nagaosa, and Y. Iwasa, "Bulk rectification effect in a polar semiconductor," *Nature Physics* **13**, 578–583 (2017).
- ⁹T. Guillet, C. Zucchetti, Q. Barbedienne, A. Marty, G. Isella, L. Cagnon, C. Vergnaud, H. Jaffrè, N. Reyren, J.-M. George, A. Fert, and M. Jamet, "Observation of large unidirectional rashba magnetoresistance in ge(111)," *Phys. Rev. Lett.* **124**, 027201 (2020).
- ¹⁰P. He, S. M. Walker, S. S.-L. Zhang, F. Y. Bruno, M. S. Bahramy, J. M. Lee, R. Ramaswamy, K. Cai, O. Heinonen, G. Vignale, F. Baumberger, and H. Yang, "Observation of out-of-plane spin texture in a srtio₃(111) two-dimensional electron gas," *Phys. Rev. Lett.* **120**, 266802 (2018).
- ¹¹G. L. J. A. Rikken, J. Fölling, and P. Wyder, "Electrical magnetochiral anisotropy," *Phys. Rev. Lett.* **87**, 236602 (2001).
- ¹²F. Pop, P. Auban-Senzier, E. Canadell, G. L. J. A. Rikken, and N. Avarvari, "Electrical magnetochiral anisotropy in a bulk chiral molecular conductor," *Nature Communications* **5**, 3757 (2014).
- ¹³V. Krstić, S. Roth, M. Burghard, K. Kern, and G. L. J. A. Rikken, "Magneto-chiral anisotropy in charge transport through single-walled carbon nanotubes," *The Journal of Chemical Physics* **117**, 11315–11319 (2002).
- ¹⁴T. Furukawa, Y. Watanabe, N. Ogasawara, K. Kobayashi, and T. Itou, "Current-induced magnetization caused by crystal chirality in nonmagnetic elemental tellurium," *Phys. Rev. Res.* **3**, 023111 (2021).
- ¹⁵M. Sakano, M. Hirayama, T. Takahashi, S. Akebi, M. Nakayama, K. Kuroda, K. Taguchi, T. Yoshikawa, K. Miyamoto, T. Okuda, K. Ono, H. Kumigashira, T. Ideue, Y. Iwasa, N. Mitsuishi, K. Ishizaka, S. Shin, T. Miyake, S. Murakami, T. Sasagawa, and T. Kondo, "Radial spin texture in elemental tellurium with chiral crystal structure," *Phys. Rev. Lett.* **124**, 136404 (2020).
- ¹⁶C. Niu, G. Qiu, Y. Wang, Z. Zhang, M. Si, W. Wu, and P. D. Ye, "Gate-tunable strong spin-orbit interaction in two-dimensional tellurium probed by weak antilocalization," *Phys. Rev. B* **101**, 205414 (2020).
- ¹⁷V. Edelstein, "Spin polarization of conduction electrons induced by electric current in two-dimensional asymmetric electron systems," *Solid State Communications* **73**, 233–235 (1990).
- ¹⁸F. Calavalle, M. Suárez-Rodríguez, B. Martín-García, A. Johansson, D. C. Vaz, H. Yang, I. V. Maznichenko, S. Ostanin, A. Mateo-Alonso, A. Chuvalin, I. Mertig, M. Gobbi, F. Casanova, and L. E. Hueso, "Gate-tunable and chirality-dependent charge-

to-spin conversion in tellurium nanowires,” *Nature Materials* **21**, 526–532 (2022).

¹⁹Q. Shao, P. Li, L. Liu, H. Yang, S. Fukami, A. Razavi, H. Wu, K. Wang, F. Freimuth, Y. Mokrousov, M. D. Stiles, S. Emori, A. Hoffmann, J. Åkerman, K. Roy, J.-P. Wang, S.-H. Yang, K. Garello, and W. Zhang, “Roadmap of spin–orbit torques,” *IEEE Trans. Magn.* **57**, 1–39 (2021).

²⁰C. Niu, S. Huang, N. Ghosh, P. Tan, M. Wang, W. Wu, X. Xu, and P. D. Ye, “Tunable circular photogalvanic and photovoltaic effect in 2d tellurium with different chirality,” *Nano Letters* **23**, 3599–3606 (2023), pMID: 37057864, <https://doi.org/10.1021/acs.nanolett.3c00780>.

²¹M. Suárez-Rodríguez, B. Martín-García, F. Calavalle, S. S. Tsirkin, I. Souza, F. de Juan, A. Fert, M. Gobbi, L. E. Hueso, and F. Casanova, “Symmetry origin and microscopic mechanism of electrical magnetochiral anisotropy in tellurium,” *Phys. Rev. B* **111**, 024405 (2025).

²²B. Ma, M. Xie, L. Zhang, S. Liu, G. Ye, X. Yang, Y. Liu, F. Chu, Y. Liu, X. Zeng, X. Lu, and X. Wang, “Weyl node–participated magnetoresistance and nonreciprocal transport in two-dimensional tellurene nanostructures,” *ACS Applied Nano Materials* **7**, 9012–9019 (2024).

²³M. Weiler, M. Althammer, F. D. Czeschka, H. Huebl, M. S. Wagner, M. Opel, I.-M. Imort, G. Reiss, A. Thomas, R. Gross, and S. T. B. Goennenwein, “Local charge and spin currents in magnetothermal landscapes,” *Phys. Rev. Lett.* **108**, 106602 (2012).

²⁴Z. Hua, C. Niu, S. Joy, P. Tan, G. Shi, H. Liu, J. Guo, D. Graf, P. Ye, C. Lewandowski, and P. Xiong, “Interplay of orbital and spin magnetization in trigonal tellurium,” (2025), arXiv:2507.14292 [cond-mat.mtrl-sci].

²⁵P. Fontana, V. Velasco, C. Niu, P. D. Ye, P. V. Lopes, K. E. M. de Souza, M. V. O. Moutinho, C. Lewenkopf, and M. B. S. Neto, “Quantum geometry and the electric magnetochiral anisotropy in noncentrosymmetric polar media,” *Phys. Rev. Lett.* **135**, 106602 (2025).